Inorganic Chemistry

ARTICLE

pubs.acs.org/IC

Dual Coordination Modes of Ethylene-Linked NP2 Ligands in Cobalt(II) and Nickel(II) Iodides

Qingchen Dong,[†,‡] Michael J. Rose,[*,†] Wai-Yeung Wong,[*,‡] and Harry B. Gray[*,†]

[†]Beckman Institute, Division of Chemistry and Chemical Engineering, California Institute of Technology, Pasadena, California 91125, United States

[‡]Institute of Molecular Functional Materials (Areas of Excellence Scheme, University Grants Committee, Hong Kong) and Department of Chemistry and Centre for Advanced Luminescence Materials, Hong Kong Baptist University, Waterloo Road, Hong Kong, P.R. China

Supporting Information

ABSTRACT:

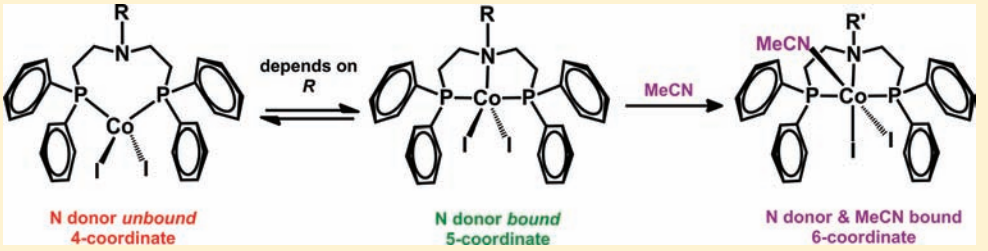

Here we report the syntheses and crystal structures of a series of cobalt(II) and nickel(II) complexes derived from $_{R}$**NP2** ligands (where **R** = OMe_{Bz}, H_{Bz}, Br_{Bz}, Ph) bearing ethylene linkers between a single N and two P donors. The Co^{II} complexes generally adopt a tetrahedral configuration of general formula $[(NP2)Co(I)_2]$, wherein the two phosphorus donors are bound to the metal center but the central N-donor remains unbound. We have found one case of structural isomerism within a single crystal structure. The Co^{II} complex derived from $_{Bz}$**NP2** displays dual coordination modes: one in the tetrahedral complex $[(_{Bz}NP2)Co(I)_2]$; and the other in a square pyramidal variant, $[(_{Bz}NP2)Co(I)_2]$. In contrast, the Ni^{II} complexes adopt a square planar geometry in which the P(Et)N(Et)P donors in the ligand backbone are coordinated to the metal center, resulting in cationic species of formula $[(_{R}NP2)Ni(I)]^+$ with iodide as counterion. All Ni^{II} complexes exhibit sharp ^1H and ^{31}P spectra in the diamagnetic region. The Co^{II} complexes are high-spin ($S = 3/2$) in the solid state as determined by SQUID measurements from 4 to 300 K. Solution electron paramagnetic resonance (EPR) experiments reveal a high-spin/low-spin Co^{II} equilibrium that is dependent on solvent and ligand substituent.

INTRODUCTION

Complexes containing late transition metals bound to phosphine donors have found application in a wide variety of industrial transformations and synthetic methodologies. Phosphorus ligands are of interest because they stabilize low oxidation states ($M^{II/I}$) that are active species in many catalytic cycles, and cobalt phosphines promote ethylene polymerization[1] and hydroformylation reactions.[2−4] Synthetically, there is ongoing interest in substituting palladium with more earth abundant metals such as nickel in C−C bond forming reactions.[5−7] Chelating trisphosphines bearing different anionic heteroatoms have been employed to shed light on ligand field effects for both anionic and neutral phosphines.

In the case of mixed phosphorus- and nitrogen-containing ligands, the additional functionality of an N-donor can allow the metal center to access a greater range of oxidation states than with phosphines alone. For example, cobalt and nickel complexes derived from pyridine-containing phosphine ligands often are more efficient ethylene polymerization catalysts.[1,8] Other investigators have used multidentate ligands bearing groups presenting "mismatched" donor strengths, as in those containing a wider variety of hard (N,O) and soft (P,S) donors.[9] Inclusion of nitrogen atoms in predominantly phosphine-based ligands has led to the development of efficient dihydrogen (H_2) evolution and oxidation catalysts containing both nickel and cobalt.[10] In each case, researchers recognized that the structural and coordination properties of a chosen ligand to a given metal center dictate the reactivity and magnetic properties of the resulting complex.

Three main types of $\mathbf{P_xN_y}$ ligands differ on the basis of structural flexibility and linker type.[11] In the case of the pyridine-based **PMP** ligand (Scheme 1), the structural rigidity of the pyridine ring enforces binding of the N-donor to the metal

Received: June 7, 2011
Published: September 13, 2011

ACS Publications © 2011 American Chemical Society

Scheme 1

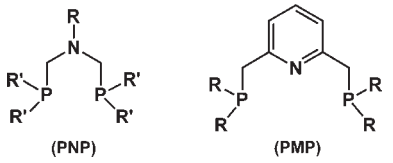

center.[8,12,13] Coordination of the P- and N-donors in **PMP** results in 5-membered ring chelates that are thermodynamically stable. For example, Rieger and co-workers prepared trigonal bipyramidal complexes $[(PMP)Co^{II}(Cl)_2]$ and $[(PMP)Fe^{II}(Cl)_2]$ in which the entire P−N−P donor set binds to the metal centers.

In contrast, the ligand **PNP** contains a methylene linker between the N- and P-atoms, which disfavors simultaneous coordination of the three donor atoms. DuBois and co-workers synthesized several Ni^{II} complexes derived from ligands of general formula $\mathbf{R_1P\text{-}N(R_2)\text{-}PR_1}$ (R_1 = Et; R_2 = Me, *n*Bu). The resulting structures adopt slightly distorted square planar geometries that display only P-coordination, while the nitrogen remains unbound. More recent work utilizing Co^{II} led to the isolation of $[(PNP)Co^{II}(MeCN)_3]$,[14,15] which also excludes the N-donor from the coordination sphere. Further work using methylene-linked cyclic ligands (**P2N2**) produced complexes in which phosphorus atoms are bound to Ni^{II} and Co^{II} centers.

Here we report work on complexes of **NP2** ligands that retain the stable 5-membered chelates found in **PMP** but impart structural flexibility by using ethylene linkers instead of a rigid pyridyl moiety (Scheme 2). Hii and co-workers found that metalation of **NP2** ligands ($_R$**NP2**; R = ^{t}Bu, Ph, 4-OMeC$_6$H$_4$) with Pd^{II} salts afforded N-bound complexes $[(_R\underline{NP2})Pd^{II}(Cl)_2]$, whereas treatment with a Pd^0 starting material produced only P-bound $[(_R\underline{NP2})Pd(dba)]$ (as determined by ^{31}P shifts).[16] Of interest is whether ligation/deligation of the N-donor is attributable to electronic factors associated with the change in oxidation state $Pd^{II}\rightarrow Pd^0$, or to a simple geometric preference of square planar Pd^{II} for the N-donor.

Scheme 2

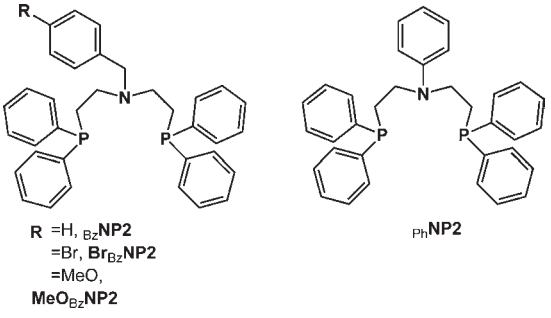

We have investigated **NP2** complexes of two transition metals *in the same oxidation state* (Ni^{II} and Co^{II}) that typically adopt different coordination geometries (square planar and tetrahedral, respectively). Here we report that **NP2** ligands with *para*-substituted benzylamines and aniline as N-substituent can adopt dual binding motifs when bound to Co^{II}, designated $\underline{NP2}$ and $\underline{NP2}$, where the donor atoms are underlined. We have explored the solid and solution state properties of the Co^{II} complexes by X-ray, superconducting quantum interference device (SQUID), and electron paramagnetic resonance (EPR) methods. The corresponding Ni^{II} complexes are all square planar with $\underline{NP2}$ coordination.

EXPERIMENTAL SECTION

Reagents and General Procedures. Benzylamine, bromobenzylamine, 2-bromoethanol and phosphorus tribromide (PBr_3) were used as received from Sigma-Aldrich. The anyhydrous metal salts cobalt(II) iodide and nickel(II) iodide also were obtained from Sigma-Aldrich, while diphenylphosphine (Ph_2PH) was from Strem. The PNP ligand $^{Ph2}P(^{Ph}N)P^{Ph2}$ was synthesized according to a published procedure.[17] Solvents (MeCN, THF, Et_2O, toluene and hexane) were obtained from a solvent purification system employing the Grubbs method,[18] while acetone from J.T. Baker was used without further purification. Deuterated solvent ($CDCl_3$) was from Cambridge Isotopes. Reactions with diphenylphosphine, metalations with CoI_2 and NiI_2, and crystallizations were performed under dry, inert N_2 atmosphere in a glovebox.

Syntheses of the Ligands. *N,N-bis(2-hydroxyethyl)-4-methoxybenzylamine.* Batches of 4-methoxybenzylamine (5.29 g, 38.5 mmol), 2-bromoethanol (10.6 g, 84.7 mmol) and excess triethylamine (20 mL) were dissolved together in 30 mL of toluene, and the mixture was allowed to reflux for 5 h. After cooling, the solvent was removed in vacuo, and tetrahydrofuran (THF) was added to the flask to dissolve the desired species. The flask was placed at −20 °C to precipitate the $NEt_3\cdot HBr$ completely. After filtration, the product was collected by evaporating the solvent. Yield: 6.94 g (80%). ^{1}H NMR in $CDCl_3$ (δ from TMS, in ppm): δ 7.30−6.83 (m, 4 H); 3.79 (s, 2 H, Ar−CH_2-N); 3.61 (t, 4 H, N(CH_2CH$_2$OH)$_2$); 2.69 (t, 4 H, (NCH$_2$CH_2OH)$_2$); 2.49 (m, 2 H, N(CH$_2$CH$_2$O*H*)$_2$).

N,N-bis(2-bromoethyl)-4-methoxybenzylamine. The bis-hydroxy starting material (4.00 g, 17.8 mmol) from the previous step was dissolved in 50 mL of CH_2Cl_2, and the solution was cooled to 0 °C in an ice bath and brought under N_2 atmosphere. To this stirred solution was added PBr_3 (3.40 mL, 35.6 mmol) dropwise via syringe over the course of 20 min. During the next 2 h, the reaction temperature was maintained at 0 °C, and a sticky yellow precipitate was observed. The reaction was allowed to come to room temperature over 2 h. Next, the reaction was quenched by addition of 10 mL of water at 0 °C, and then neutralized to pH 7 with a saturated solution of Na_2CO_3. The organic layer was separated from the aqueous phase, dried over $MgSO_4$, and the solvent removed under reduced pressure. The product was purified via silica gel chromatography and eluted with CH_2Cl_2:hexanes (1:1) to afford a colorless oil. Yield: 4.40 g (71%). ^{1}H NMR in $CDCl_3$ (δ from TMS, in ppm): δ 7.26−6.82 (m, 4 H, Ar-*H*); 3.80 (s, 3 H, *Me*O); 3.65 (s, 2 H, Ar−CH_2-N); 3.32 (t, 4 H, N(CH_2CH$_2$Br)$_2$); 2.94 (t, 4 H, (NCH$_2$CH_2Br)$_2$).

N,N-bis(2-(diphenylphosphino)ethyl)-4-methoxybenzylamine {MeO_{Bz}NP2}. Under N_2 atmosphere in a glovebox, diphenylphosphine (0.880 g, 4.70 mmol) was diluted in 15 mL of THF and treated with 0.580 g (5.18 mmol) of ^{t}BuOK. The clear Ph_2PH solution turned to a bright red color upon addition of base, and the mixture was stirred at room temperature for 30 min. Separately, bis-bromo-4-methoxybenzylamine (0.790 g, 2.25 mmol) described above was dissolved in 5 mL of degassed THF. The deprotonated phosphine was brought to 0 °C, and the solution of dibromo-species was added dropwise over the course of 10 min. After the addition was complete, the solution was colorless, and the reaction was allowed to come to ambient temperature over the next 5 h. Next, 5 mL of water were added to quench the reaction, and the THF was removed in vacuo; 30 mL of CH_2Cl_2 were added and the organic layers collected and dried over $MgSO_4$, then the

dx.doi.org/10.1021/ic201213c |*Inorg. Chem.* 2011, 50, 10213–10224

solvent was removed under reduced pressure. The product was purified on silica gel using CH_2Cl_2 EtOAc/hexanes (1:10), and isolated as a white solid. Yield: 1.01 g (80%). ^{1}H NMR in $CDCl_3$ (δ from TMS, in ppm): δ 7.34−6.74 (m, 24 H, Ar-*H*); 3.79 (s, 3 H, *Me*O); 3.49 (s, 2 H, Ar−C*H*$_2$-N); 2.59−2.51 (m, 4 H, N(C*H*$_2$CH$_2$PPh$_2$)$_2$); 2.11−2.06 (m, 4 H, (NCH$_2$C*H*$_2$PPh$_2$)$_2$). ^{31}P NMR in $CDCl_3$ (δ from H_3PO_4): δ −20.15 (s). ^{13}C NMR in $CDCl_3$ (δ from TMS, in ppm): δ 158.5 (s, 1 C), 138.5 (d, 4 C), 132.6 (d, 8 C), 131.1 (s, 1 C), 130.0 (s, 2 c), 128.5 (s, 4 C), 128.3 (d, 8 C), 113.6 (s, 2 C), 57.3 (s, 1 C), 55.3 (s, 1 C), 49.2 (d, 2 C), 25.4 (d, 2 C).

N,N-bis(2-hydroxyethyl)benzylamine. A large batch of benzyl bromide (7.14 g, 41.7 mmol) was dissolved in 30 mL of acetone. Separately, diethanolamine (4.82 g, 45.9 mmol) was dissolved in 5 mL of acetone and added to a stirred solution of the benzyl bromide, followed by addition of solid Na_2CO_3 (4.42 g, 41.7 mmol). The solution was refluxed for 4 h and cooled to room temperature. Next, acetone was removed and 20 mL of water were added to dissolve the NaBr, followed by extraction with 30 mL of CH_2Cl_2. The organic layer was dried over $MgSO_4$, and the solvent evaporated to dryness. The resulting oil was washed with 2 × 10 mL of hexane, affording the desired product as a clear oil. Yield: 6.76 g (83%). ^{1}H NMR in $CDCl_3$ (δ from TMS, in ppm): δ 7.33−7.29 (m, 5 H, Ar-*H*); 3.70 (s, 2 H, Ar−C*H*$_2$-N); 3.61 (t, 4 H, N(C*H*$_2$CH$_2$OH)$_2$); 2.71 (t, 4 H, (NCH$_2$C*H*$_2$OH)$_2$); 2.44 (m, 2 H, N(CH$_2$CH$_2$O*H*)$_2$).

N,N-bis(2-bromoethyl)benzylamine. The reaction of bis-hydroxy-4-benzylamine (5.65 g, 29.0 mmol) with 2 equiv of PBr_3 (5.70 mL, 60.5 mmol) was performed as described above, and the crude product was isolated according to the same extraction procedure. The product was purified via silica gel chromatography and eluted with CH_2Cl_2: hexanes (1:2) to afford a colorless oil. Yield: 8.70 g (75%). ^{1}H NMR in $CDCl_3$ (δ from TMS, in ppm): δ 7.34−7.28 (m, 5 H, Ar-*H*); 3.73 (s, 2 H, Ar−C*H*$_2$-N); 3.34 (t, 4 H, N(C*H*$_2$CH$_2$Br)$_2$); 2.97 (t, 4 H, (NCH$_2$C*H*$_2$Br)$_2$).

N,N-bis(2-(diphenylphosphino)ethyl)benzylamine {$_{Bz}$*NP2*}. The reaction of the bis-bromoethyl-benzylamine (2.25 g, 5.64 mmol) with 2.10 g of Ph_2PH (11.3 mmol) and 1.41 g of ^{t}BuOK (12.4 mmol) in 30 mL of THF was carried out according to the procedure for **MeO$_{Bz}$NP2** as stated above. The product was purified on silica gel using CH_2Cl_2 as solvent, and isolated as a white solid. Yield: 2.30 g (77%). ^{1}H NMR in $CDCl_3$ (δ from TMS, in ppm): δ 7.33−7.23 (m, 25 H, Ar-*H*); 3.56 (s, 2 H, Ar−C*H*$_2$-N); 2.62−2.57 (m, 4 H, N(C*H*$_2$CH$_2$PPh$_2$)$_2$); 2.13−2.08 (m, 4 H, (NCH$_2$C*H*$_2$PPh$_2$)$_2$). ^{31}P NMR in $CDCl_3$ (δ from H_3PO_4): δ ppm −20.34 (s). ^{13}C NMR in $CDCl_3$ (δ from TMS, in ppm): δ 25.4 (d, 2 C), 49.3 (d, 2 C), 58.0 (s, 1 C), 126.9 (s, 1 C), 128.1−128.9 (m, 18 C), 132.6 (d, 8 C), 138.5 (d, 2 C), 139.1 (s, 1 C).

N,N-bis(2-hydroxyethyl)-4-bromobenzylamine. The reaction of 4-bromobenzylbromide (3.00 g, 12.0 mmol) with 1 equiv of diethanolamine and Na_2CO_3 was carried out under the same conditions as described above. Yield: 2.73 g (83%). ^{1}H NMR in $CDCl_3$ (δ from TMS, in ppm): δ 7.46, 7.43 (d, 2 H, Ar-*H*); 7.28, 7.21 (d, 2 H, Ar-*H*); 3.65 (s, 2 H, Ar−C*H*$_2$-N); 3.62 (t, 4 H, N(C*H*$_2$CH$_2$OH)$_2$); 2.69 (t, 4 H, (NCH$_2$C*H*$_2$OH)$_2$).

N,N-bis(2-bromoethyl)-4-bromobenzylamine. The reaction of bis-hydroxy-4-bromobenzylamine (1.50 g, 5.49 mmol) with 2 equiv of PBr_3 (2.07 mL, 11.0 mmol) was performed as described above, and the crude product was isolated according to the same extraction procedure. The product was purified via silica gel chromatography and eluted with CH_2Cl_2:hexanes (1:2) to afford a colorless oil. Yield: 1.71 g (78%).^{1}H NMR in $CDCl_3$ (δ from TMS, in ppm): δ 7.46, 7.44 (d, 2 H, Ar-*H*); 7.25, 7.22 (d, 2 H, Ar-*H*); 3.68 (s, 2 H, Ar−C*H*$_2$-N); 3.34 (t, 4 H, N(C*H*$_2$CH$_2$Br)$_2$); 2.95 (t, 4 H, (NCH$_2$C*H*$_2$Br)$_2$).

N,N-bis(2-(diphenylphosphino)ethyl)-4-bromobenzylamine {*Br$_{Bz}$NP2*}. The reaction of the bis-bromoethyl-benzylamine (1.03 g, 2.58 mmol) with 0.960 g of Ph_2PH (5.15 mmol) and 0.640 g of ^{t}BuOK (5.68 mmol) in 30 mL of THF was carried out, and the product purified as described above. Yield: 1.20 g (76%). ^{1}H NMR in $CDCl_3$ (δ from TMS, in ppm): δ 7.35−7.27 (m, 22 H, Ar-*H*); 7.09, 7.07 (d, 2 H, Ar-*H*); 3.48 (s, 2 H, Ar−C*H*$_2$-N); 2.59−2.51 (m, 4 H, N(C*H*$_2$CH$_2$PPh$_2$)$_2$); 2.12−2.09 (m, 4 H, (NCH$_2$C*H*$_2$PPh$_2$)$_2$). ^{31}P NMR in $CDCl_3$ (δ from H_3PO_4): δ ppm −20.34 (s). ^{13}C NMR in $CDCl_3$ (δ from TMS, in ppm): δ 25.4 (d, 2 C), 49.3 (d, 2 C), 57.4 (s, 1 C), 120.6 (s, 1 C), 128.5 (m, 12 C), 130.5 (s, 2 C), 131.2 (s, 2 C), 132.6 (d, 8 C), 138.3 (m, 5 C).

N,N-bis(2-bromoethyl)phenylamine. The reaction of *N*-phenyl-diethanolamine (5.00 g, 27.6 mmol) with 2 equiv of PBr_3 (5.40 mL, 55.2 mmol) was performed as described above, and the crude product was isolated according to the same extraction procedure. The product was purified via silica gel chromatography and eluted with CH_2Cl_2: hexanes (1:2) to afford a colorless oil. Yield: 6.60 g (78%). ^{1}H NMR in $CDCl_3$ (δ from TMS, in ppm): δ 6.67−7.30 (m, 5 H, Ar-*H*); 3.78 (t, 4 H, N(C*H*$_2$CH$_2$Br)$_2$); 3.46 (t, 4 H, (NCH$_2$C*H*$_2$Br)$_2$).

N,N-bis(2-(diphenylphosphino)ethyl)phenylamine {$_{Ph}$*NP2*}. The reaction of the bis-bromoethyl-phenylamine (1.69 g, 5.50 mmol) with 2.05 g of Ph_2PH (11.0 mmol) and 1.36 g of ^{t}BuOK (12.1 mmol) in 30 mL of THF was carried out, and the product purified as described above. Yield: 2.13 g (75%). ^{1}H NMR in $CDCl_3$ (δ from TMS, in ppm): δ 7.43−6.33 (m, 25 H, Ar-*H*); 3.38−3.30 (m, 4 H, N(C*H*$_2$CH$_2$PPh$_2$)$_2$); 2.30−2.25 (m, 4 H, (NCH$_2$C*H*$_2$PPh$_2$)$_2$). ^{31}P NMR in $CDCl_3$ (δ from H_3PO_4): δ ppm −21.35 (s). ^{13}C NMR in $CDCl_3$ (δ from TMS, in ppm): δ 25.9 (d, 2 C), 47.7 (d, 2 C), 112.3 (s, 2 C), 116.2 (s, 1 C), 128.6 (m, 12 C), 129.3 (s, 2 C), 132.7 (d, 8 C), 137.9 (d, 4 C), 146.7 (s, 1 C).

Syntheses of the Co^{II} and Ni^{II} Complexes. All Co^{II} and Ni^{II} complexes were prepared and recrystallized by procedures similar to those employed for [($_{Bz}$NP2)Co(I)$_2$] (**Co-2**) and [($_{Bz}$NP2)Ni(I)]I (**Ni-2**), as detailed below.

[($_{Bz}$NP2)Co(I)$_2$] (***Co-2***). The $_{Bz}$NP2 ligand (0.200 g, 0.380 mmol) was dissolved in 10 mL of degassed THF. Separately, anhydrous CoI_2 (0.118 g, 0.380 mmol) was slurried in 3 mL of THF and added dropwise to the stirred solution of the NP2 ligand at room temperature; this immediately generated a dark brown color. The solution was stirred for 12 h, and then filtered to remove a small amount of unreacted CoI_2. The brown solution was layered with 3 volumes of degassed hexane and after 3−4 days, orange-green crystals suitable for X-ray diffraction were obtained. Yield: 312 mg (90%). UV/vis in THF, λ in nm (ε in M^{-1} cm^{-1}): 778 (220), 714 (300), 486 sh (440), 363 (1 900). Anal. Calcd. for $C_{35}H_{35}NP_2CoI_2$: C 49.79, H 4.18, N 1.66; found: C 50.45, H 4.02, N 1.92.

[(MeO$_{Bz}$NP2)Co(I)$_2$] (***Co-1***). Reaction of the methoxy-appended MeO$_{Bz}$NP2 ligand (0.20 g, 0.36 mmol) with 0.11 g of CoI_2 (0.35 mmol) was performed as described above; the product crystallized from THF/hexane after several days. Yield: 277 mg (88%). UV/vis in THF, λ in nm (ε in M^{-1} cm^{-1}): 778 (630), 715 (750), 487 sh (890), 363 (2 330). Anal. Calcd. for $C_{36}H_{37}NOP_2CoI_2$: C 49.45, H 4.27, N 1.60; found: C 48.83, H 4.77, N 1.45.

[(Br$_{Bz}$NP2)Co(I)$_2$] (***Co-3***). Reaction of the bromine-appended Br$_{Bz}$NP2 ligand (0.50 g, 0.82 mmol) with 0.26 g of CoI_2 (0.82 mmol) was performed as described above; the product crystallized from THF/hexane after 1−2 days. Yield: 700 mg (93%). UV/vis in THF, λ in nm (ε in M^{-1} cm^{-1}): 778 (790), 718 (910), 486 sh (990), 363 (2 630). Anal. Calcd. for $C_{35}H_{34}NBrP_2CoI_2$: C 45.53, H 3.71, N 1.52; found: C 44.93, H 3.76, N 1.71.

[($_{Ph}$NP2)Co(I)$_2$] (***Co-4***). Reaction of $_{Ph}$NP2 ligand (0.15 g, 0.29 mmol) with 0.09 g of CoI_2 (0.29 mmol) was performed as described above; the product crystallized from THF/hexane after 1−2 days. Yield: 220 mg (90%). UV/vis in THF, λ in nm (ε in M^{-1} cm^{-1}): 363 (950). Anal. Calcd. for $C_{34}H_{33}NP_2CoI_2$: C 49.18, H 4.01, N 1.69; found: C 49.28, H 3.82, N 1.49.

[P(N$_{Ph}$)P)Co(I)$_2$] (***Co-PNP***). Reaction of the PNP type of ligand P(N$_{Ph}$)P (0.30 g, 0.61 mmol) with 0.19 g of CoI_2 (0.61 mmol) was

Table 1. Crystal Data and Refinement Parameters for NP2-Co^{II} Complexes

	Co-1	Co-2	Co-3	Co-4
empirical formula	$C_{36}H_{37}NOP_2CoI_2$	$C_{35}H_{35}NP_2CoI_2 \cdot C_4H_8O$	$C_{35}H_{34}NP_2BrCoI_2$	$C_{34}H_{33}NP_2CoI_2$
FW	874.34	916.41	923.21	830.28
color	green	green	green	dark green
habit	needle	blade	plate	block
size (mm)	0.38 × 0.10 × 0.07	0.20 × 0.10 × 0.07	0.19 × 0.14 × 0.07	0.31 × 0.23 × 0.11
T (*K*)	100(2)	100(2)	100(2)	100(2)
wavelength (Å)	0.71073	0.71073	0.71073	0.71073
lattice system	orthorhombic	monoclinic	triclinic	orthorhombic
space group	$P2_12_12_1$	$P2_1/c$	$P\bar{1}$	$P2_12_12_1$
a (Å)	9.2880(4)	9.1301(5)	9.5306(4)	11.7095(6)
b (Å)	13.5281(5)	14.38705(7)	11.7513(5)	14.2950(7)
c (Å)	27.2546(11)	28.7247(14)	15.7593(7)	19.3910(11)
α (deg)	90	90	98.758(2)	90
β (deg)	90	94.000(2)	93.890(2)	90
γ (deg)	90	90	101.072(2)	90
V (Å^3)	3424.5(2)	3763.9(3)	1703.35(13)	3237.6(3)
Z	4	4	2	4
d_{calc} (g/cm^3)	1.696	1.617	1.800	1.703
μ (mm^{-1})	2.427	2.212	3.609	2.560
GOF on F^2	1.548	1.663	1.433	1.268
final *R* indices	*R1* = 0.0241	*R1* = 0.0287	*R1* = 0.0280	*R1* = 0.0224
[$I > 2\sigma(I)$]	w*R2* = 0.0376	w*R2* = 0.0411	w*R2* = 0.0381	w*R2* = 0.0316
R indices	*R1* = 0.0283	*R1* = 0.0427	*R1* = 0.0445	*R1* = 0.0306
all data	w*R2* = 0.0381	w*R2* = 0.0424	w*R2* = 0.0393	w*R2* = 0.0326

performed as described above; the product crystallized from THF/hexane after 3−4 days. Yield: 400 mg (82%). UV/vis in THF, λ in nm (ε in M^{-1} cm^{-1}): 781 (630), 718 (790), 487 (1 170), 363 sh (3 170). Anal. Calcd. for $C_{32}H_{29}NP_2CoI_2$: C 47.91, H 3.64, N 1.75; found: C 47.58, H 3.79, N 1.77.

[($_{Bz}$NP2)Ni(I)]I (***Ni-2***). The $_{Bz}$NP2 ligand (0.15 g, 0.28 mmol) was dissolved in 5 mL of degassed THF. Separately, anhydrous NiI_2 (0.088 g, 0.28 mmol) was dissolved in 5 mL of THF by vigorously stirring and then added dropwise to the stirred solution of the NP2 ligand at room temperature; this immediately generated a red-violet color. The solution was stirred for 12 h, and then filtered to remove the unreacted NiI_2. The red-violet solution was layered with 3 volumes of degassed hexane and after 3−4 days, red crystals suitable for X-ray diffraction were obtained. Yield: 210 mg (89%). ^{1}H NMR in $CDCl_3$ (δ from TMS, in ppm): δ 8.48−8.46 (m, 2 H, Ar-*H*); 7.86−7.42 (m, 23 H, Ar-*H*); 4.41 (s, 2 H, Ar−C*H*$_2$-N); 3.96 (m, 2 H, N(C*H*$_2$CH$_2$PPh$_2$)$_2$); 3.26−3.21 (m, 2 H, N(C*H*$_2$CH$_2$PPh$_2$)$_2$); 2.98−2.94 (m, 2 H, N(CH$_2$C*H*$_2$PPh$_2$)$_2$); 2.71−2.64 (m, 2 H, (NCH$_2$C*H*$_2$PPh$_2$)$_2$). ^{31}P NMR in $CDCl_3$ (δ from H_3PO_4): δ ppm 35.65 (s). UV/vis in THF, λ in nm (ε in M^{-1} cm^{-1}): 341 sh (4 230), 294 sh (8 780). Anal. Calcd. for $C_{35}H_{35}NP_2NiI_2$: C 49.80, H 4.18, N 1.66; found: C 49.97, H 3.99, N 1.80.

[(MeO$_{Bz}$NP2)Ni(I)]I (***Ni-1***). Reaction of the methoxy-appended MeO$_{Bz}$NP2 ligand (83 mg, 0.15 mmol) with 46 mg of NiI_2 (0.15 mmol) was performed as described above; the product crystallized from THF/hexane after 3−4 days. Yield: 110 mg (83%). ^{1}H NMR in $CDCl_3$ (δ from TMS, in ppm): δ 8.36, 8.33 (d, 2 H, Ar-*H*); 7.82−7.44 (m, 20 H, Ar-*H*); 6.92, 6.90 (d, 2 H, Ar-*H*); 4.34 (s, 2 H, Ar−C*H*$_2$-N); 3.90 (m, 2 H, N(C*H*$_2$CH$_2$PPh$_2$)$_2$); 3.81 (s, 3 H, *Me*O); 3.17 (m, 2 H, N(C*H*$_2$CH$_2$PPh$_2$)$_2$); 2.92 (m, 2 H, (NCH$_2$C*H*$_2$PPh$_2$)$_2$); 2.74−2.67 (m, 2 H, (NCH$_2$C*H*$_2$PPh$_2$)$_2$). ^{31}P NMR in $CDCl_3$ (δ from H_3PO_4): δ ppm 35.47 (s). UV/vis in THF, λ in nm (ε in M^{-1} cm^{-1}): 337 sh (3 310), 294 sh (6 630). Anal. Calcd. for $C_{36}H_{37}NOP_2NiI_2$: C 49.46, H 4.27, N 1.60; found: C 49.05, H 4.15, N 1.48.

[(Br$_{Bz}$NP2)Ni(I)]I (***Ni-3***). Reaction of the bromine-appended Br$_{Bz}$NP2 ligand (0.20 g, 0.33 mmol) with 0.11 g of NiI_2 (0.33 mmol) was performed as described above; the product crystallized from THF/hexane after 1−2 days. Yield: 270 mg (88%). ^{1}H NMR in $CDCl_3$ (δ from TMS, in ppm): δ 8.74, 8.44 (d, 2 H, Ar-*H*); 7.82−7.43 (m, 22 H, Ar-*H*); 4.41 (s, 2 H, Ar−C*H*$_2$-N); 4.04 (m, 2 H, N(C*H*$_2$CH$_2$PPh$_2$)$_2$); 3.22 (m, 2 H, N(C*H*$_2$CH$_2$PPh$_2$)$_2$); 2.91−2.74 (m, 2 H, (NCH$_2$-C*H*$_2$PPh$_2$)$_2$); 2.70−2.17 (m, 2 H, (NCH$_2$C*H*$_2$PPh$_2$)$_2$). ^{31}P NMR in $CDCl_3$ (δ from H_3PO_4): δ ppm 35.46 (s). UV/vis in THF, λ in nm (ε in M^{-1} cm^{-1}): 338 sh (2 660), 294 sh (7 140). Anal. Calcd. for $C_{35}H_{34}NBrP_2NiI_2$: C 45.54, H 3.71, N 1.52; found: C 45.30, H 3.83, N 1.40.

[($_{Ph}$NP2)Ni(I)]I (***Ni-4***). Reaction of the $_{Ph}$NP2 ligand (190 mg, 0.36 mmol) with 120 mg of NiI_2 (0.37 mmol) was performed as described above; the product crystallized from THF/hexane after several days. Yield: 260 mg (85%). ^{1}H NMR in $CDCl_3$ (δ from TMS, in ppm): δ 8.09, 8.07 (d, 2 H, Ar-*H*); 7.64−7.43 (m, 23 H, Ar-*H*); 4.62 (m, 3 H, N(C*H*$_2$C*H*$_2$PPh$_2$)$_2$); 3.46 (m, 3 H, (NC*H*$_2$C*H*$_2$PPh$_2$)$_2$); 2.68−2.64 (m, 2 H, (NCH$_2$C*H*$_2$PPh$_2$)$_2$). ^{31}P NMR in $CDCl_3$ (δ from H_3PO_4): δ ppm 36.06 (s). UV/vis in THF, λ in nm (ε in M^{-1} cm^{-1}): 360 (1 610), 294 (3 720). Anal. Calcd. for $C_{34}H_{33}NP_2NiI_2$: C 49.20, H 4.01, N 1.69; found: C 48.66, H 4.12, N 1.52.

[(P(N$_{Ph}$)P)Ni(I)$_2$] (***Ni-PNP***). Reaction of the ^{Ph}P(N$_{Ph}$)P^{Ph} ligand (0.30 g, 0.61 mmol) with 0.19 g of NiI_2 (0.61 mmol) was performed as described above. Yield: 410 mg (84%). ^{1}H NMR in $CDCl_3$ (δ from TMS, in ppm): δ ppm, 9.25 (br m, 2 H); 7.37 (br d, 9 H); 7.06 (br m, 8 H); 6.82 (br m, 2 H); 6.13 (br m, 4 H); 4.68 (br s, 4 H). ^{31}P NMR in $CDCl_3$ (δ from H_3PO_4): δ ppm −5.11 (s). Anal. Calcd. for $C_{32}H_{29}NP_2NiI_2$: C 47.92, H 3.64, N 1.75; found: C 48.36, H 3.61, N 1.97.

dx.doi.org/10.1021/ic201213c |*Inorg. Chem.* 2011, 50, 10213–10224

Table 2. Selected Bond Distances (Å) and Bond Angles (deg) from Crystal Structures of the Cobalt Complexes[a]

	Co-1	Co-2 ($P2_1/c$)	Co-2 (DFT)	Co-2′	Co-3	Co-3 (DFT)	Co-4
Co−P1	2.3529(3)	2.3563(4)	2.339	2.1945(5)	2.3761(3)	2.310[b]	2.3511(3)
Co−P2	2.3572(3)	2.3566(4)	2.333	2.2228(5)	2.3990(3)	2.354[b]	2.3420(3)
Co−I1	2.57678(19)	2.5703(2)	2.569	2.6023(3)	2.5766(17)	2.566	2.58189(16)
Co−I2	2.54416(17)	2.5599(2)	2.583	2.7480(4)	2.5650(17)	2.585	2.54249(15)
Co---N	3.690	3.674	3.658	2.0769(18)	3.675	3.633	3.684
P1−Co−P2	113.307(11)	114.376(14)	114.68	161.57(2)	115.373(10)	115.65	113.829(9)
P−Co−I (avg)	107.284(9)	106.696(12)	107.12	95.994(16)	106.594(8)	106.57	106.651(8)
I1−Co−I2	114.400(6)	115.503(8)	115.40	95.229(12)	115.006(6)	114.96	116.386(5)

[a] Also included for comparison are DFT-optimized (6-31G*[b]/PW91) bond distances for **Co-2** and **Co-3**. [b] Denotes a difference of greater than 0.05 Å.

Table 3. Crystal Data and Refinement Parameters for the NP2-Ni^{II} Complexes

	Ni-1	Ni-2	Ni-3	Ni-4
empirical formula	$[C_{36}H_{37}NOP_2INi]^+I^-$	$[C_{35}H_{35}INP_2Ni]^+I^- \cdot CH_2Cl_2$	$[C_{35}H_{34}NP_2BrINi]^+I^-$	$[C_{34}H_{33}NP_2INi]^+I^- \cdot C_4H_8O$
FW	874.12	929.02	922.99	902.17
color	purple	deep purple	dark purple	red
habit	block	blade	block	block
size (mm)	0.28 × 0.27 × 0.18	0.20 × 0.18 × 0.10	0.21 × 0.18 × 0.15	0.29 × 0.28 × 0.15
T (K)	100(2)	100(2)	100(2)	100(2)
wavelength (Å)	0.71073	0.71073	0.71073	0.71073
lattice system	triclinic	monoclinic	triclinic	triclinic
space group	$P\bar{1}$	$P2_1/n$	$P\bar{1}$	$P\bar{1}$
a (Å)	11.9939(5)	8.9712(4)	11.9678(6)	9.7033(3)
b (Å)	12.7222(5)	24.7251(10)	12.1991(12)	12.3287(4)
c (Å)	12.9714(9)	16.2706(7)	13.2965(7)	15.5781(5)
α (deg)	105.152(2)	90	103.056(4)	86.4940(10)
β (deg)	100.967(2)	93.804(2)	108.995(3)	87.5220(10)
γ (deg)	110.363(2)	90	102.700(4)	89.1920(10)
V (Å^3)	1702.42(15)	3601.1(3)	1695.0(2)	1858.24(10)
Z	2	4	2	2
d_{calc} (g/cm^3)	1.705	1.714	1.808	1.612
μ (mm^{-1})	2.507	2.517	3.693	2.299
GOF on F^2	2.336	1.675	2.002	2.081
final R indices	$R1$ = 0.0282	$R1$ = 0.0299	$R1$ = 0.0329	$R1$ = 0.0282
$[I > 2\sigma(I)]$	w$R2$ = 0.0497	w$R2$ = 0.0414	w$R2$ = 0.0520	w$R2$ = 0.0586
R indices	$R1$ = 0.0400	$R1$ = 0.0459	$R1$ = 0.0475	$R1$ = 0.0348
all data	w$R2$ = 0.0502	w$R2$ = 0.0426	w$R2$ = 0.0529	w$R2$ = 0.0601

X-ray Crystallography. Crystals were mounted on a glass fiber using Paratone oil, and then placed on the diffractometer under a stream of N_2 at 100 K. Refinement of F^2 against all reflections: the weighted R-factor (wR) and goodness of fit (S) were based on F^2, conventional R-factors (R) were based on F, with F set to zero for negative F^2. The threshold expression $F^2 > 2\sigma(F^2)$ was used only for calculating R-factors(gt) and was not relevant to the choice of reflections for refinement. Diffraction intensity data were collected on a Bruker Kappa APEX II diffractometer equipped with a MoKα X-ray source, and data were collected using APEX2 v2009.7−0; the data reduction program SAINT-plus v7.66A was used. Details of the data collections and refinements are given in Tables 1 and 3.

Magnetism. Magnetic susceptibilities for **Co-1**, **Co-2**, **Co-3**, and **Co-4** were recorded at 5000 G using a Quantum Designs SQUID magnetometer controlled by MPMSR2 software. Data points acquired from 4 to 300 K were corrected for diamagnetic contributions (Pascal's constants).[19] The output was converted to effective magnetic moment (μ_{eff}) and plotted as BM (μ_B) versus temperature (K).

Spectroscopy. The ^{1}H, ^{13}C, and ^{31}P NMR spectra were recorded on a Varian Mercury 300 MHz spectrometer, and chemical shifts were referenced to TMS (^{1}H, ^{13}C) or H_3PO_4 (^{31}P). EPR spectra were recorded on a Bruker EMX Biospin spectrometer at 20 K using a Gunn diode microwave source. UV/vis spectra were obtained at 298 K using a Cary 50 spectrophotometer.

Density Functional Theory (DFT) Calculations. Geometry optimization on the crystal structure coordinates as well as orbital calculations were performed using the pure functional PW91[20] and the 6-31G* basis set (6-311G* for iodine) in the Firefly software package.[21] Orbitals were visualized using MacMolPlt,[22] and spin density plots were generated using gOpenMol.[23]

RESULTS AND DISCUSSION

Syntheses. We have synthesized a series of NP2 ligands with a flexible {P-CH_2CH_2-N-CH_2CH_2-P} binding unit.

Scheme 3

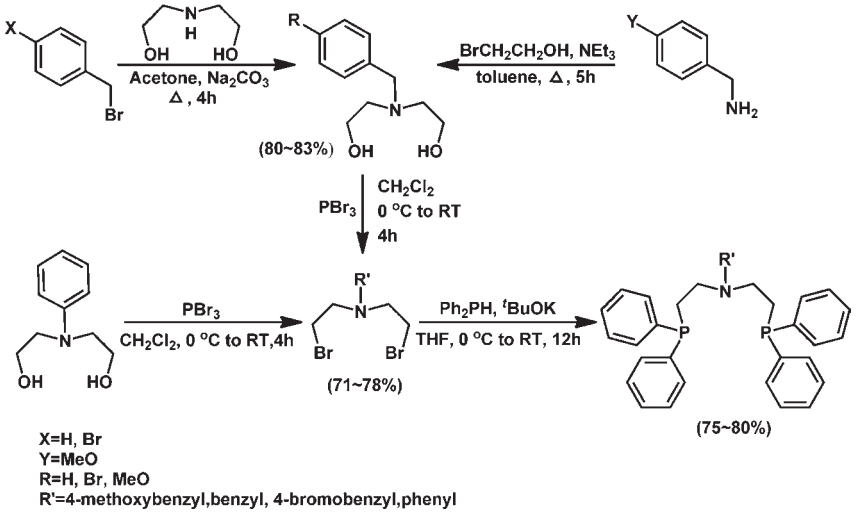

Scheme 4

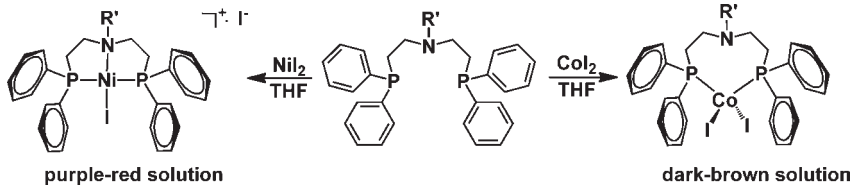

Many reported PNP compounds were synthesized via a Mannich-type reaction with the corresponding phosphine, amines, and CH_2O, thereby providing methylene linked ligands. We opted for a different approach to prepare ethylene-bridged ligands. Our first targeted compound was the bis-hydroxyethyl derivative. Reaction of benzylbromide (or 4-bromobenzylbromide) with diethanolamine in acetone (Na_2CO_3 as base) afforded the corresponding bis-hydroxyethyl derivatives in excellent yields. Alternatively, the −OMe appended bis-hydroxyethyl derivative was produced by refluxing a mixture of 4-methoxylbenzylamine, 2-bromoethanol, and NEt_3 in toluene for 5 h; *N*-phenyldiethanolamine is commercially available. Subsequent activation of the alcohols with PBr_3 generated the brominated derivatives (71−78%), which upon disubstitution with diphenylphosphine (^{t}BuOK as base) afforded the **NP2** ligands as air-stable, white solids in very good yield (75−80%, Scheme 3).

Metalation of 1 equiv of a given **NP2** ligand with anhydrous CoI_2 in THF at room temperature afforded a dark brown solution (Scheme 4). Crystals of the resulting Co^{II} complexes of general formula $[(_RNP2)Co(I)_2]$ were isolated in nearly quantitative yield (81−92%). The Ni^{II} species also were prepared by the reaction of 1 equiv of the NP2 ligands with anhydrous NiI_2 in THF under inert atmosphere. The resulting violet solutions generated copious amounts of purple solid that could be recrystallized from THF/hexane. X-ray crystallography (see below) identified these complexes as the cationic species of general formula $[(_RNP2)Ni(I)]^+$ in very good yield (82−90%). The Ni^{II} complexes exhibit sharp ^1H and ^{31}P NMR spectra in the diamagnetic region, consistent with an $S = 0$ ground state.

Crystal Structures of the Cobalt Complexes. The Co^{II} center in each of the complexes of general formula $[(_RNP2)Co(I)_2]$ is coordinated by two phosphino-P donors provided by bidentate **NP2** as well as two iodide ions, adopting a tetrahedral geometry (Figure 1; selected bond lengths and bond angles are in Table 2.) Crystal data and refinement parameters for **NP2**-Co^{II}complexes are collected in Table 1. The overall structures of these four-coordinate Co^{II} complexes are pseudotetrahedral with P1−Co−P2 (113.307°−115.373°), P−Co−I (avg) (106.594°−107.284°) and I1−Co−I2 (114.400°−116.386°) bond angles that deviate only slightly from ideal values. The Co−P bond lengths (2.3511(3)−2.3761(3) Å) are longer than those observed in complexes bearing a bidentate P2N2 ligand, such as $[(P^{Ph}{}_2N^{Ph}{}_2)Co(MeCN)_3]^{2+}$ (2.198(5) Å) or $[(P^{Ph}{}_2N^{Ph}{}_2)2Co(Cl)]^+$ (2.2133(8) and 2.2368(8) Å).[15] They also are longer than those in [(PhBP3)-Co(I)] ($BP3^- = PhB(CH_2P(Ph)_2)_3^-$) (2.200(2), 2.206(2), and 2.282(2) Å).[24] The Co−I bond lengths (avg Co−I = 2.565 Å) are longer than those observed in [(PhBP3)Co(I)] (2.488(1) Å) and $[(PhBP^{iPr}3)Co(I)]$ (2.540(1) Å), which may be attributable to the different number of coordinated iodides in each case. The distances between the Co^{II} center and the unbound N donor lie in the narrow range 3.674−3.690 Å.

The related **P2N2** and **PNP** ligands are methylene linked. In a P-N-P bonded chelate, these ligands would generate two unfavorable 4-membered rings among the {Co-P-CH_2-N-(Co)} atoms. The **NP2** ligands, with an ethylene linker between the phosphorus and nitrogen atoms, could form two ideal {Co-P-CH_2-CH_2-N-(Co)} 5-membered rings; *in most cases* (vide infra) the nitrogen remains unbound, indicating that the tetrahedral cobalt center prefers phosphorus ligation.

dx.doi.org/10.1021/ic201213c |*Inorg. Chem.* 2011, 50, 10213–10224

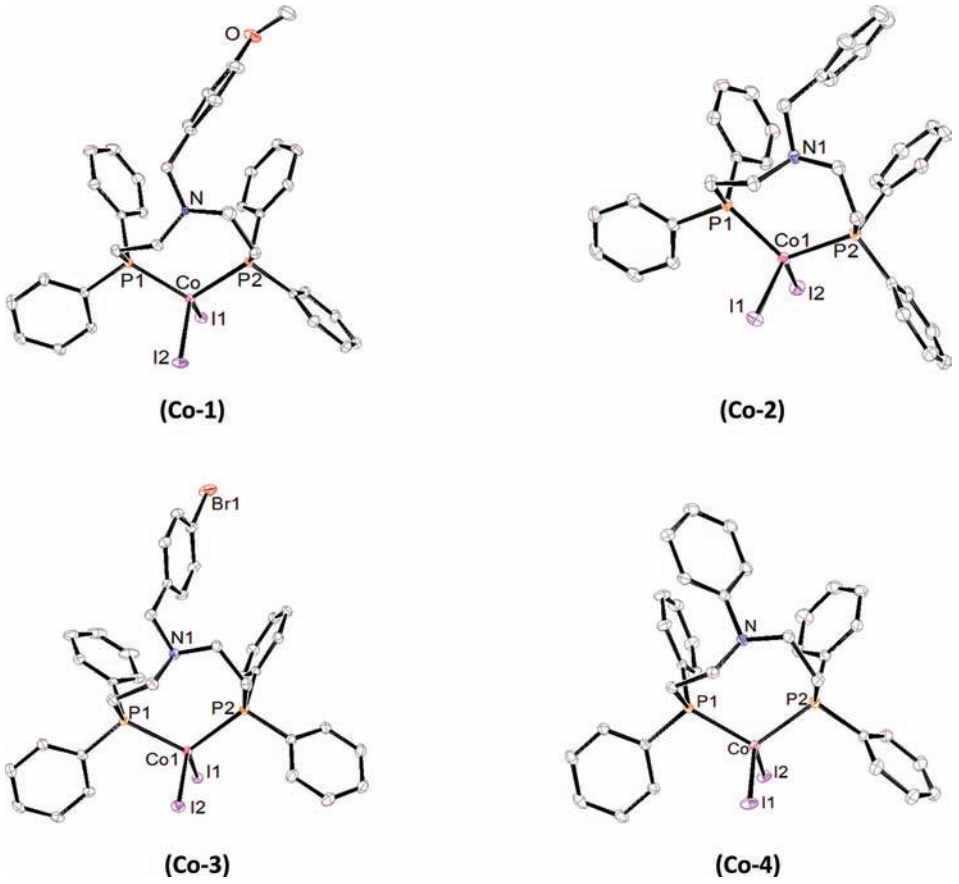

Figure 1. ORTEP diagrams (50% thermal ellipsoids): $[(MeO_{Bz}NP2)Co(I)_2]$ (**Co-1**); $[(_{Bz}NP2)Co(I)_2]$ (**Co-2**); $[(Br_{Bz}NP2)Co(I)_2]$ (**Co-3**); $[(_{Ph}NP2)Co(I)_2]$ (**Co-4**).

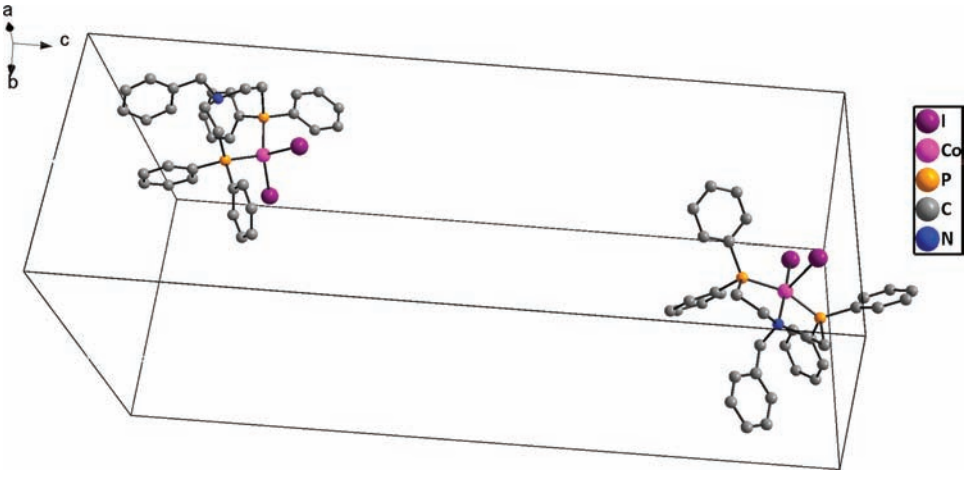

Figure 2. Ball and stick diagram of the asymmetric part of the unit cell (*Cc* crystal structure) containing $[(_{Bz}NP2)Co(I)_2]$ structural conformers: **Co-2**, tetrahedral (left side); **Co-2′**, square pyramidal (right side).

One notable exception is the five-coordinate Co^{II} complex obtained from the reaction of CoI_2 with 2 equiv of $_{Bz}$**NP2**. In this case, the complex crystallized in a different space group (*Cc*), in contrast to the crystal structure that contains only the tetrahedral complex described above ($P2_1/c$). Figure 2 displays the asymmetric part of the *Cc* unit cell, which contains two structural conformers denoted **Co-2** (tetrahedral) and **Co-2′** (square pyramidal). In the case of **Co-2′** (right side), the cobalt center adopts a square pyramidal geometry because of binding of the benzylamino-*N* donor. The I^- occupies the apical position, while the other I^-, two phosphorus atoms and nitrogen reside in the basal plane. The Co−N bond length (2.0769(18) Å) is much shorter than {Co- - -N} in the tetrahedral Co complexes (∼3.7 Å), but slightly longer than the $Co-N_{MeCN}$ bond lengths

dx.doi.org/10.1021/ic201213c |*Inorg. Chem.* 2011, 50, 10213–10224

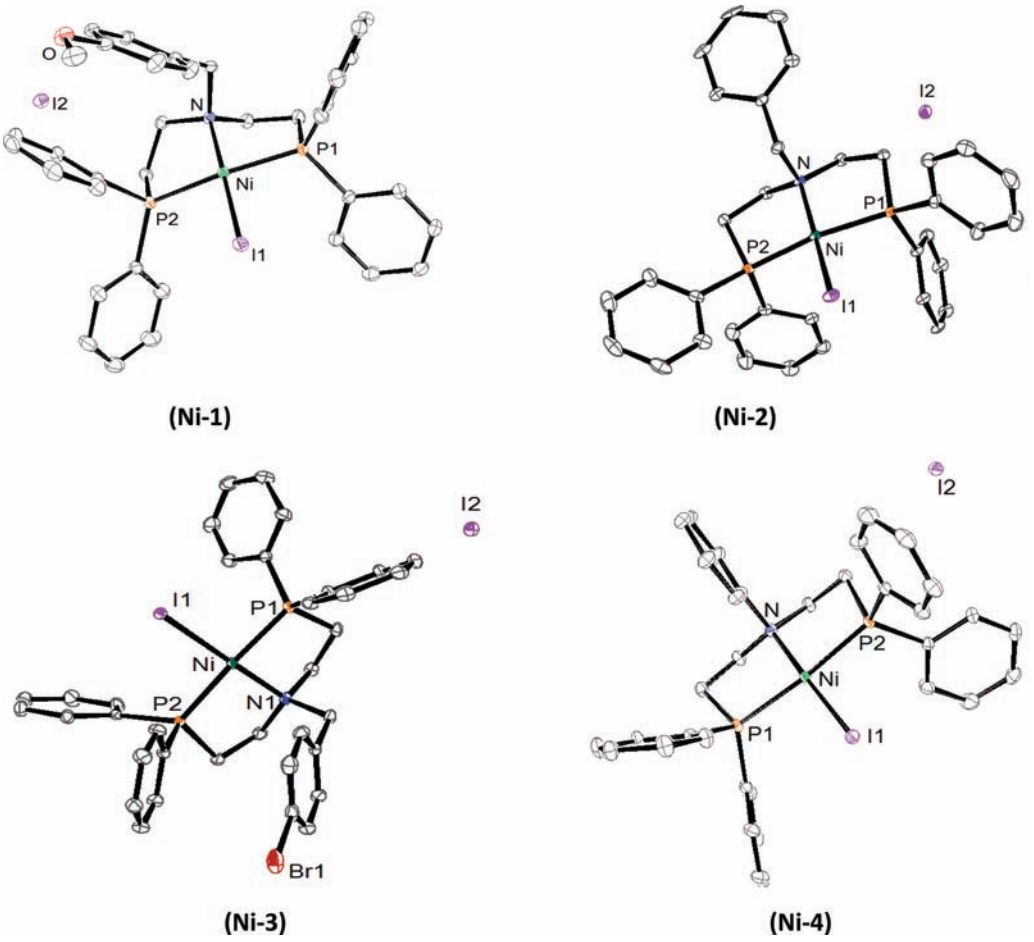

Figure 3. ORTEP diagrams (50% thermal ellipsoids): [(MeO_{Bz}NP2)Ni(I)]I (**Ni-1**); [($_{Bz}$NP2)Ni(I)]I (**Ni-2**); [(Br_{Bz}NP2)Ni(I)]I (**Ni-3**); [($_{Ph}$NP2)Ni(I)]I (**Ni-4**).

Table 4. Selected Bond Distances (Å) and Bond Angles (deg) from Crystal Structures of Ni^{II} Complexes

	Ni-1	Ni-2	Ni-3	Ni-4	Ni-PNP
Ni−P1	2.2139(2)	2.2039(3)	2.2062(4)	2.2264(4)	2.1833(3)
Ni−P2	2.1916(2)	2.2319(3)	2.2039(4)	2.2181(4)	2.1760(3)
Ni−I1	2.4739(2)	2.4744(16)	2.4871(3)	2.4870(2)	2.53658(15)
Ni−I2					2.53083(14)
Ni−N	2.0051(7)	1.9864(8)	1.9887(11)	1.9911(12)	3.771
P1−Ni−P2	164.876(10)	157.662(13)	175.916(15)	173.670(16)	93.381(10)
P1−Ni−I1	94.251(7)	92.936(8)	91.784(11)	94.559(11)	176.719(9)
P1−Ni−I2					174.479(9)
N−Ni−I1	177.22(2)	166.37(3)	174.92(3)	178.26(3)	

in [Co($P^{Ph}_2N^{Ph}_2$)(CH_3CN)$_3$](BF_4)$_2$ (1.952, 2.078, 1.943 Å)[15] or [Co($P^{tBu}_2N^{Bz}_2$)(CH_3CN)$_3$](BF_4)$_2$ (1.961, 1.955, 2.059 Å).[14] The Co−P distances are both shortened (2.1945(5) and 2.2228(5) Å) once the N-donor is bound. On the other hand, the Co−I bond lengths are elongated (2.6023(3) and 2.7480(4) Å). The structure of the *Cc* tetrahedral **Co-2** is nearly identical with that in the $P2_1/c$ crystal.

Crystal Structures of the Nickel Complexes. Table 3 shows crystal data and refinement parameters for the **NP2**-Ni^{II} complexes. ORTEP diagrams for the four square planar $_R$**NP2**-Ni^{II} complexes are shown in Figure 3; selected bond angles and bond distances are in Table 4. The N-donor in $_R$**NP2** is bound to Ni^{II}, even in the case of $_{Ph}$**NP2** (**Ni-4**). In each case, one I^- ligand occupies the fourth coordination site, while the other I^- is an outer coordination counterion. **Ni-1**, **Ni-3**, and **Ni-4** exhibit P1−Ni−P2 and N−Ni−I1 angles in the range 164.876(10)−178.26(3)°; **Ni-2** exhibits a more distorted square planar geometry, with P1−Ni−P2 and N−Ni−I1 angles of 157.662(13)° and 166.37(3)°, respectively. The dihedral angle P1−Ni−I1/P2−Ni−N in **Ni-2** is 24.95°. The Ni−P bonds (2.2039(3) and 2.2319(3) Å) in **Ni-2** are elongated by comparison to the other distorted Ni complexes. The Ni−P bond lengths (**Ni-1** = 2.203, **Ni-2** = 2.221, **Ni-3** = 2.205, **Ni-4** = 2.222 Å) are very close to those in [(PNP)Ni(dmpm)](BF_4)$_2$ (Ni−P_{avg} ≈ 2.21 Å).[25]

ORTEP diagrams for **Ni-PNP** and **Co-PNP** complexes are shown in Figure 4 (for crystal data and refinement parameters see Supporting Information, Table S1). In contrast to **Ni-1** to **Ni-4**, only P-donors are coordinated in **Ni-PNP**, as the aniline N-donor is approximately 3.8 Å away from the metal center. The Ni−P bonds in **Ni-PNP** (Ni−P1 = 2.1833(3), Ni−P2 = 2.1760(3) Å) are shorter than the average Ni−P length in **Ni-1**−**Ni-4** (Ni−P1 = 2.2126(3), Ni−P2 = 2.2114(3) Å), most likely because of the "pinched" geometry in the methylene-linked PNP. As a result, the Ni−I1 bond lengths in **Ni-PNP** (2.53658(15) Å) are longer than the average Ni−I1 distance in **Ni-1**−**Ni-4** (2.4806(6) Å), likely attributable to a stronger *trans* effect of the more closely bonded P-donors. We suggest that

dx.doi.org/10.1021/ic201213c |*Inorg. Chem.* 2011, 50, 10213–10224

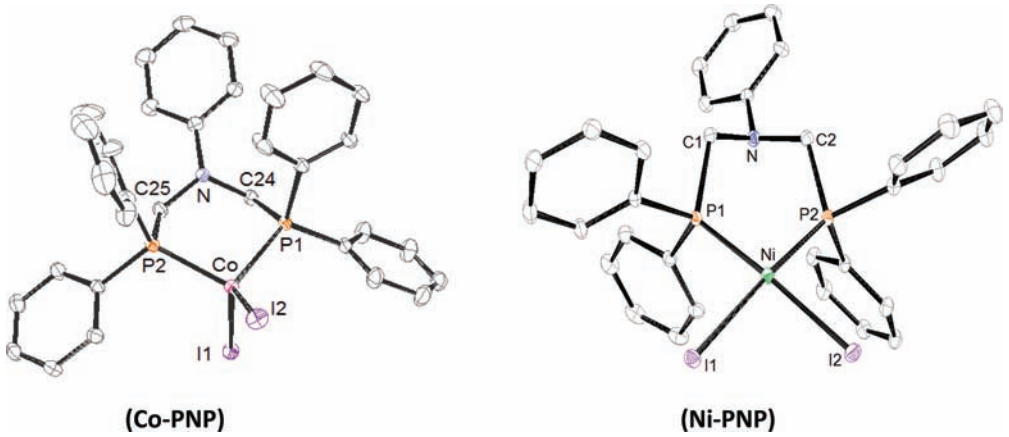

Figure 4. ORTEP diagrams (50% thermal ellipsoids): $[(P(N_{Ph})P)Co(I)_2]$ (**Co-PNP**); $[(P(N_{Ph})P)Ni(I)_2]$ (**Ni-PNP**).

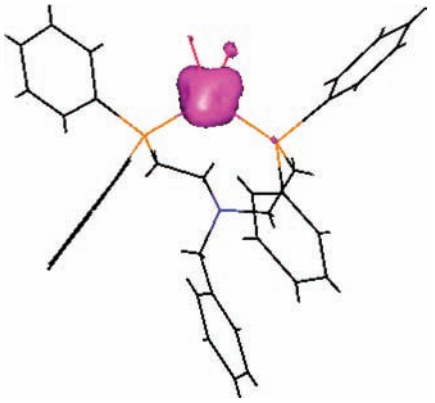

Figure 5. DFT (6-31G*/PW91) spin density plot for the S = 3/2 ground state of the geometry optimized **Co-2** structure.

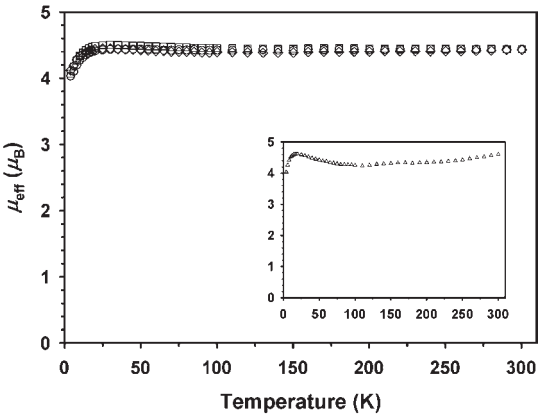

Figure 6. Plots of μ_{eff} (BM) versus T: $[(OMe_{Bz}NP2)Co(I)_2]$, **Co-1**, (◇); $[(Br_{Bz}NP2)Co(I)_2]$, **Co-3**, (○); $[(_{Ph}NP2)Co(I)_2]$, **Co-4**, (□). Inset: $[(_{Bz}NP2)Co(I)_2]$, **Co-2**, (Δ).

the nitrogen atom of the NP2 ligand acts as a "claw" to pull Ni^{II} back, thus forming two 5-membered rings when the nitrogen is bound to the metal center. The corresponding Co^{II} structure is unremarkable, as **Co-PNP** exhibits a similar P-only coordination mode as in **Ni-PNP** and **Co-1**−**Co-4**. Thus, the dual coordination modes of ethylene-linked $_R$**NP2** ligands are not observed in P-only complexes containing **PNP**.

DFT Calculations. We performed DFT calculations on **Co-2** and **Co-3** as model compounds. Geometry optimization at the 6-31G*/PW91 (S = 3/2) level afforded bond distances and bond angles very similar to those found in the crystal structure, with no differences in bond lengths >0.03 Å (Table 2). DFT calculations on **Co-3** gave similar results, although the Co−P bonds in the calculation (2.310, 2.354 Å) were significantly shorter than those in the crystal (2.3761(3), 2.3990(3) Å); the Co−I bonds, however, were in good agreement (diff <0.02 Å). In the DFT calculation, the S = 3/2 ground state of **Co-2** is approximately 25 kcal/mol more stable than the S = 1/2 state, as observed in some tetrahedral Co^{II} complexes bearing anionic phosphine ligands.[24] The spin density of **Co-2** (shown in Figure 5) is consistent with that expected for a nearly ideal T_d system, a result in accord with SQUID data (vide infra). It was necessary to establish unambiguously the S = 3/2 ground state in the solid state by SQUID and DFT calculations in light of unexpected EPR results (vide infra).

Magnetic Susceptibilities. We determined magnetic susceptibilities for **Co-1**, **Co-2**, **Co-3**, and **Co-4** over the temperature range 4 to 300 K using SQUID magnetometry (Figure 6). Complexes **Co-3** and **Co-4** exhibit little variation in μ_{eff} in the range 25 to 300 K. At low temperature (4 K), the magnetic moments are 4.03 μ_B and 4.07 μ_B, respectively, in reasonable agreement with the spin-only value (3.87 μ_B) for an S = 3/2 system. Such an S = 3/2 ground state is typically observed for tetrahedral Co^{II} complexes.[26−29]

The magnetic data for **Co-2** are more difficult to interpret: μ_{eff} decreases slowly from 300 (4.61) to 110 K (4.24 μ_B), then increases from 110 to 20 K. Nonetheless, the 4 K magnetic moment for **Co-2** of 4.04 μ_B is nearly identical with those for **Co-3** and **Co-4**. The data for **Co-2** were obtained using crystals from the 1:1 ratio ($_{Bz}$**NP2**:Co) reaction (the $P2_1/c$ *tetrahedral-only* structure). It is possible that deviation from ideal Curie−Weiss behavior is due to trace quantities of *Cc* crystals (obtained from the 2:1 ratio reaction of $_{Bz}$**NP2**:Co) that contain structural conformers **Co-2**/**Co-2′** (vide supra). We conclude that the $_R$**NP2**-Co^{II} complexes are high-spin (S = 3/2) in the solid state, as expected for tetrahedral and pseudotetrahedral structures.[30]

EPR. We recorded EPR spectra for **Co-1** and **Co-3** in the solid state at 4 K (Supporting Information, Figure S1). In each case, the spectrum is dominated by high-spin Co^{II} signals near $g \approx 6$ in accord with the SQUID data. Peters and co-workers also reported consistent SQUID and *solid state* EPR results for both

dx.doi.org/10.1021/ic201213c |*Inorg. Chem.* 2011, 50, 10213–10224

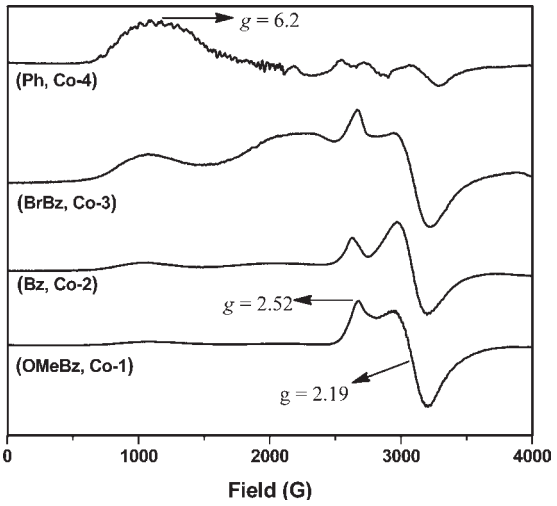

Figure 7. EPR spectra for Co^{II} complexes in frozen THF at 20 K (from top to bottom): $[(_{Ph}NP2)Co(I)_2]$ (**Co-4**); $[(Br_{Bz}NP2)Co(I)_2]$ (**Co-3**); $[(_{Bz}NP2)Co(I)_2]$ (**Co-2**); $[(MeO_{Bz}NP2)Co(I)_2]$ (**Co-1**). Microwave frequency, 9.453 GHz; field modulation, 20 G; microwave power, 2 mW; frequency modulation, 100 kHz.

$\{[PhBP_3]Co(\mu\text{-}Br)\}_2$ and $\{[PhBP_3]Co(\mu\text{-}Br)\}_2$.[24] The 20 K EPR spectra of the four Co^{II} complexes in THF are shown in Figure 7: **Co-4** exhibits a primary feature at $g = 6.2$ (Figure 7, top spectrum) typical for distorted tetrahedral $S = 3/2$ systems.

There is a systematic increase in the intensities of $g \approx 2$ features with increasing N-donor strength (Ph-*N* < BrBz-*N* < Bz-*N* < OMeBz-*N* in **Co-4** < **Co-3** < **Co-2** < **Co-1**), and a concomitant decrease in the broad high-spin system near $g \approx 6$. As a result, the EPR spectrum of $[(OMe_{Bz}NP2)Co(I)_2]$ (**Co-1**) at the opposite end of the donor strength trend is dominated by a rhombic, low-spin signal with primary features at $g = 2.52$ and 2.19. Such a spectrum is consistent with low-spin ($S = 1/2$) Co^{II} with vastly different axial ligands (e.g., anionic vs neutral; or neutral vs unoccupied site). The lineshapes of the low-spin signals in **Co-1**, **Co-2**, and **Co-3** closely follow those of a related square pyramidal Co^{II} phosphine complex $[(PP3)Co(MeCN)]^{2+}$ ($g = 2.11$).[31] Similar features were observed for low-spin complexes $[Co(P^{Ph}2N^{Ph}2)_2(CH_3CN)](BF_4)_2$ ($g = 2.11$) and $[Co(dppe)_2(CH_3CN)](BF_4)_2$ ($g = 2.20$) that also are square pyramidal.[15,30,31] Thus, it is likely that $[(OMe_{Bz}NP2)Co(I)_2]$ (**Co-1**) has adopted a square pyramidal coordination geometry in THF.

We suggest that the two conformers exist in solution whose relative populations are influenced by the ligand substituent. Correspondingly, the EPR spectra in Figure 7 clearly show that as the *N*-substituent becomes more strongly donating, the EPR signal attributable to the square pyramidal conformer is dominant. The −OMe appended ligand strongly enforces the five-coordinate geometry of $[(OMe_{Bz}NP2)Co(I)_2]$ (**Co-1′**). In contrast, the $[(_{Ph}NP2)Co(I)_2]$ (**Co-4**) EPR spectrum is consistent *only* with a tetrahedral geometry, while those of **Co-3** and **Co-2** can be interpreted in terms of mixtures of conformers. It is apparent that subtle differences in ligand substitutent can tune the coordination modes of **NP2**-type ligands.

Frozen MeCN/tol Glass. We observed further dynamic behavior of the **NP2** ligands in EPR experiments performed in MeCN. The complex derived from the weakest N-donor, $[(_{Ph}NP2)Co(I)_2]$ (**Co-4**), displays an EPR spectrum (Figure 8, top spectrum) in MeCN/tol (3:1, 20 K) that is dominated by low-spin features ($g = 2.42$, 2.22) that are consistent with a five-coordinate geometry. The complex $[(_{Bz}NP2)Co(I)_2]$ (**Co-2**) in frozen MeCN/tol also exhibits exclusively low-spin features ($g = 2.43$, 2.22; Figure 8, bottom spectrum). In both cases, it is likely that conversion to the square pyramidal (or octahedral) conformer is facilitated by coordination of MeCN. For comparison, $[(PP3)Co(MeCN)]^{2+}$, $[Co(P^{Ph2}N^{Ph2})_2(CH_3CN)]^{2+}$, and $[Co(dppe)_2(CH_3CN)]^{2+}$ each exhibit coordinated MeCN in a square pyramidal geometry. It is well-known that M^{II} centers in octahedral or square pyramidal geometries have a strong preference for back-bonding ligands such as MeCN, CN^-, and py because of strong $\{d_\pi(M)|\pi^*(L)\}$ overlap. This is in contrast to the relatively low affinity for *tetrahedral* M^{II} centers for back-bonding ligands.

In our case, coordination of the N-donor of the **NP2** backbone is likely driven by the high stability of the two 5-membered P-N-P chelate rings that form the equatorial plane. Once a square pyramidal unit is established, MeCN could facilitate the formation of octahedral geometry bearing the **NP2** and I^- donors in the

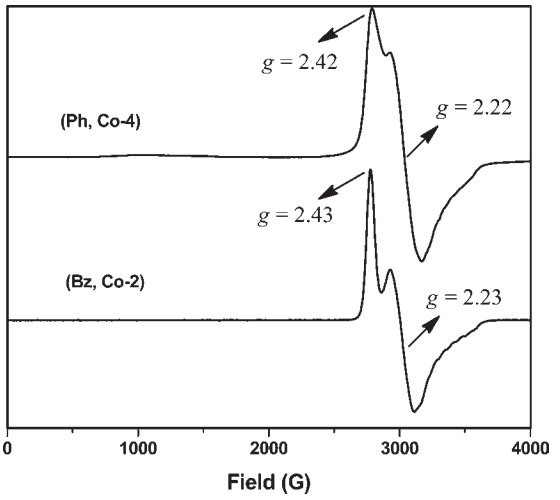

Figure 8. EPR spectra of $[(_{Bz}NP2)Co(I)_2]$ (**Co-2**) and $[(_{Ph}NP2)Co(I)_2]$ (**Co-4**) in frozen MeCN/tol glass at 20 K.

Scheme 5. Coordination Modes of NP2 Co^{II} Complexes in Solutions

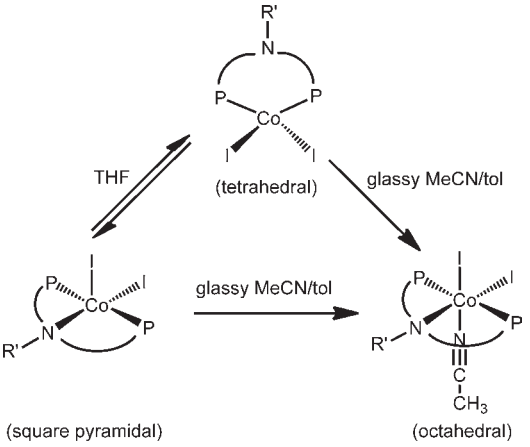

dx.doi.org/10.1021/ic201213c |*Inorg. Chem.* 2011, 50, 10213–10224

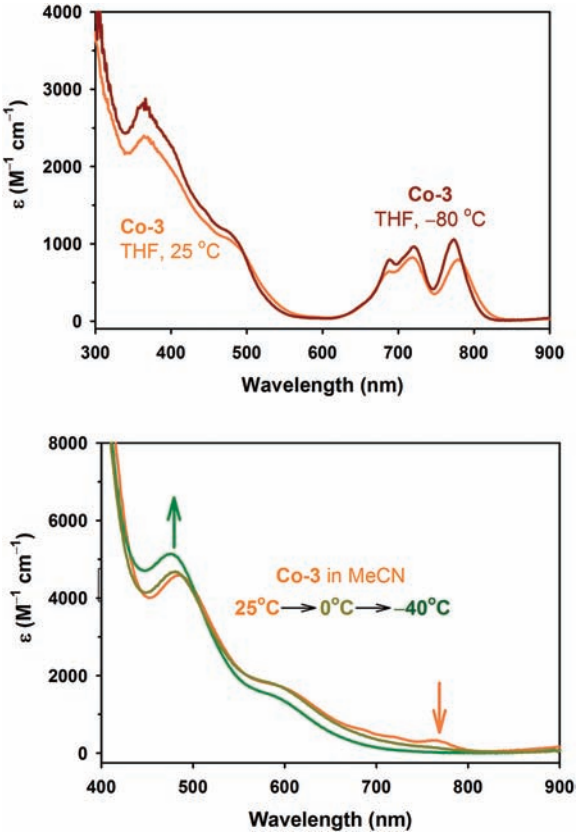

Figure 9. (Top) UV/vis spectra of **Co-3** measured in THF at 25 and −80 °C. (Bottom) UV/vis spectra of **Co-3** in MeCN at 25, 0, and −40 °C.

equatorial plane, while MeCN and the second I^- occupy axial positions (see Scheme 5). An octahedral formulation is consistent the finding that all **NP2** cobalt complexes exhibit low-spin EPR signals in MeCN. Overall, the EPR experiments illustrate the role of solvent (MeCN versus THF) in modulating the dual coordination modes of **NP2** ligands.

UV/vis Absorption Spectra. We also investigated the spin states of the cobalt complexes by UV/vis spectrophotometry in THF and MeCN. In THF solution at 25 °C, all of the complexes exhibit the following: **Co-3** exhibits peaks at 780 and 720 nm (790 and 910 M^{-1} cm^{-1}, respectively), which we assign high-spin Co^{II} LF transitions (Figure 9, top). The same solution at −80 °C exhibits slightly sharper features at 785 and 725 nm of comparable intensity, suggesting that even at this low temperature **Co-3** remains high-spin in THF. In contrast, the spectrum of **Co-3** in MeCN (25 °C) exhibits a peak near 800 nm that is much less intense (~250 M^{-1} cm^{-1}). Furthermore, as the MeCN solution of **Co-3** is cooled first to 0 °C and then −40 °C, the feature near 800 nm disappears (Figure 9, bottom), consistent with the finding that only a low-spin Co^{II} signal is observed in EPR experiments in MeCN at low temperatures (20 to 80 K). We conclude that there is a high/low-spin equilibrium (as evident in the EPR spectra) in MeCN solution, and that the low-spin state is strongly favored at lower temperatures (below 0 °C). In contrast, THF solutions of **Co-3** must be cooled to much lower temperatures (less than −80 °C) to observe even partial populations of the low-spin conformer (EPR experiments). We found similar behavior for **Co-1**, **Co-2**, and **Co-4** with slightly different high-spin/low-spin ratios that correlate with the donor strength of the ligand.

In summary, we have synthesized a series of NP2 type of ligands and corresponding Co^{II} and Ni^{II} complexes. From the crystal structures of these metal complexes, we have found that NP2 ligands exhibit dual coordination modes. The dual coordination modes are due to the geometric preference of the metal center: Co^{II} (tetrahedral) and Ni^{II} (square planar), best exhibited by the unusual crystal *Cc* structure containing **Co-2**/**Co-2′** with two conformers in a single unit cell. We intend to exploit this facile N-donor ligation/deligation property in designs of M^{II} complexes for reactions involving activation of organic substrates.

■ ASSOCIATED CONTENT

Supporting Information. Crystal structure data for all complexes (CIF files), and solid state EPR spectra of **Co-1** and **Co-3** (Figure S1). This material is available free of charge via the Internet at http://pubs.acs.org.

■ AUTHOR INFORMATION

Corresponding Author
*E-mail: mrose@caltech.edu.

■ ACKNOWLEDGMENT

This work was supported by the NSF CCI Solar Fuels Research Program (CHE-0802907). M.J.R. also received support from an NSF ACC-F postdoctoral fellowship (NSF CHE-1042009). W.Y.W. and Q.C.D. thank the Hong Kong Research Grants Council (HKBU202508), the University Grants Committee of HKSAR, China (Project No. [AoE/P-03/08]) and Hong Kong Baptist University for support. We thank Drs. Larry Henling and Michael Day for assistance in solving crystal structures, and Dr. Angelo Di Bilio for assistance in recording EPR spectra. The Bruker KAPPA APEXII X-ray diffractometer was purchased via an NSF CRIF:MU award to the California Institute of Technology (CHE-0639094).

■ REFERENCES

(1) Zhou, B.; He, R.; Xie, Z. *J. Mol. Catal A: Chem.* **2003**, *198*, 369–375.
(2) Godard, C.; Duckett, S. B.; Polas, S.; Tooze, R.; Whitwood, A. C. *Dalton Trans.* **2009**, 2496–2509.
(3) Heck, R. F.; Breslow, D. S. *J. Am. Chem. Soc.* **1961**, *83*, 1097–1102.
(4) Wood, C. D.; Garrou, P. E. *Organometallics* **1984**, *3*, 170–174.
(5) Widhalm, M.; Wimmer, P.; Klintschar, G. *J. Organomet. Chem.* **1996**, *523*, 167–178.
(6) Vechorkin, Oleg.; Csok, Z.; Scopelliti, R.; Hu, X. *Chem.—Eur. J.* **2009**, *15*, 3889–3899.
(7) Castonguay, A.; Beauchamp, A. L.; Zargarian, D. *Organometallics* **2008**, *27*, 5723–5732.
(8) Müller, G.; Klinga, M.; Leskelä, M.; Rieger, B. Z. *Anorg. Allg. Chem.* **2002**, *628*, 2839–2846.
(9) Balch, A. L.; Fossett, L. A.; Olmstead, M. M. *Inorg. Chem.* **1986**, *25*, 4526.
(10) DuBois, M. R.; DuBois, D. L. *Chem. Soc. Rev.* **2009**, *38*, 62–72.
(11) Ziessel, R. *Tetrahedron Lett.* **1989**, *30*, 463–466.
(12) Cochran, B. M.; Michael, F. E. *J. Am. Chem. Soc.* **2008**, *130*, 2786–2792.
(13) Jia, G.; Lee, H. M.; Williams, I. D.; Lau, C. P.; Chen, Y. *Organometallics* **1997**, *16*, 3941–3949.

(14) Widener, E. S.; Yang, J. Y.; Dougherty, W. G.; Kassel, W. S.; Bullock, R. M.; DuBois, M. R.; DuBois, D. L. *Organometallics* **2010**, *29*, 5390–5401.
(15) Jacobsen, G. M.; Yang, J. Y.; Twamley, B.; Wilson, A. D.; Bullock, R. M.; DuBois, M. R.; DuBois, D. L. *Energy Environ. Sci.* **2008**, *1*, 167–174.
(16) Hii, K. K.; Thornton-Pett, M. *Organometallics* **1999**, *18*, 1887–1896.
(17) Durran, S. E.; Elsegood, M. R. J.; Hawkins, N.; Smith, M. B.; Talib, S. *Tetrahedron Lett.* **2003**, *44*, 5255–5257.
(18) Pangborn, A. B.; Giardello, M. A.; Grubbs, R. H.; Rosen, R. K.; Timmers, F. J. *Organometallics* **1996**, *15*, 1518.
(19) Kahn, O. *Molecular Magnetism*; VCH Publishers: New York, 1993; pp 1−86.
(20) (a) Perdew, J. P.; Chevary, J. A.; Vosko, S. H.; Jackson, K. A.; Pederson, M.; R.; Singh, D. J.; Fiolhais, C. *Phys. Rev. B: Condens. Matter* **1993**, *48*, 4978. (b) Perdew, J. P.; Chevary, J. A.; Vosko, S. H.; Jackson, K. A.; Pederson, M. R.; Singh, D. J.; Fiolhais, C. *Phys. Rev. B: Condens. Matter* **1992**, *46*, 6671–6687.
(21) Granovsky, A. A. *Firefly*, v.7.1.G.; http://classic.chem.msu.su/gran/firefly/index.html.
(22) Bode, B. M.; Gordon, M. S. *J. Mol. Graphics* **1998**, *16*, 133–138.
(23) (a) Laaksonen, L. *J. Mol. Graphics* **1992**, *10*, 33–34. (b) Bergman, D. L.; Laaksonen, L.; Laaksonen, A. *J. Mol. Graphics* **1997**, *15*, 301–306.
(24) (a) Jenkins, D. M.; Di Bilio, A. J.; Allen, M. J.; Betley, T. A.; Peters., J. C. *J. Am. Chem. Soc.* **2002**, *124*, 15336–15350. (b) Jenkins, D. M.; Peters, J. C. *J. Am. Chem. Soc.* **2005**, *127*, 7148–7165.
(25) Curtis, C. J.; Miedaner, A.; Ciancanelli, R.; Ellis, W. W.; Noll, B. C.; DuBois, M. R.; DuBois, D. L. *Inorg. Chem.* **2003**, *42*, 216–227.
(26) Holm, R. H. *Acc. Chem. Res.* **1969**, *2*, 307–316.
(27) Cotton, F. A.; Soderberg, R. H. *J. Am. Chem. Soc.* **1962**, *84*, 872–873.
(28) Everett, G. W.; Holm, R. H. *J. Am. Chem. Soc.* **1965**, *87*, 5266–5267.
(29) Sacconi, L.; Orlandini, A.; Midollini, S. *Inorg. Chem.* **1974**, *13*, 2850–2859.
(30) Pseudotetrahedral Co^{II} complexes have been reported that have low-spin ground states. For example, $[(PhPhBP_3)Co(I)]$ (μ_{eff} = 2.67 μ_B; g = 2.20, 2.05; ref 24). However, this system displayed low-spin behavior in solid state as well (SQUID, 4−300 K), whereas our cobalt complexes exhibit high-spin S = 3/2 configuration in the ground state (see SQUID section above). Thus we rule out any possibility of a low-spin tetrahedral system in our work.
(31) DuBois, D. L.; Miedaner, A. *Inorg. Chem.* **1986**, *25*, 4642–4650.